A&A 670, L20 (2023)
https://doi.org/10.1051/0004-6361/202245530

Astronomy & Astrophysics

LETTER TO THE EDITOR

Does the virial mass drive the intra-cluster light?

Relationship between the ICL and M_{vir} from VEGAS

R. Ragusa[1,2], E. Iodice[1], M. Spavone[1], M. Montes[3,4], D. A. Forbes[5], S. Brough[6], M. Mirabile[7,8], M. Cantiello[7], M. Paolillo[1,2], and P. Schipani[1]

[1] INAF Osservatorio Astronomico di Capodimonte, Salita Moiariello 16, 80131 Napoli, Italy
e-mail: rossella.ragusa@inaf.it
[2] Università di Napoli "Federico II", Via Cinthia 21, Napoli 80126, Italy
[3] Instituto de Astrofisica de Canarias, c/ Vìa Làctea s/n, 38205 La Laguna, Tenerife, Spain
[4] Departamento de Astrofisica, Universidad de La Laguna, 38205 La Laguna, Tenerife, Spain
[5] Centre for Astrophysics and Supercomputing, Swinburne University, John Street, Hawthorn, VIC 3122, Australia
[6] School of Physics, University of New South Wales, NSW 2052, Australia
[7] INAF Osservatorio Astronomico di Teramo, Via Maggini, 64100 Teramo, Italy
[8] Gran Sasso Science Institute (GSSI), 67100 L'Aquila, Italy

Received 22 November 2022 / Accepted 12 December 2022

ABSTRACT

In this Letter, we revisit the relationship between the fraction of the intra-cluster light (ICL) as well as the virial mass and the fraction of early-type galaxies in the host halo. This exploration is based on a statistically significant and homogeneous sample of 22 groups and clusters of galaxies in the Local Universe ($z \leq 0.05$), obtained with the VST Early-type GAlaxy Survey (VEGAS). Taking advantage of the long integration time and large area of the VEGAS images, we are able to map the galaxy outskirts and ICL down to $\mu_g \geq 29$–30 mag arcsec^{-2} and out to hundreds of kpc. With this data set, we have expanded the sample of ICL measurements, doubling the previous measures available from the literature for $z \leq 0.05$. The main result of this work is the apparent lack of any significant trend between the fraction of ICL and the virial mass of the host environment, covering a wide range of virial masses ($\sim 10^{12.5} \leq M_{\rm vir} \leq 10^{15.5}\ M_{\odot}$), in full agreement with a number of theoretical studies. Since the new data points have all been derived based on the same methodology and from the same observational setup, all with comparable depths, the large observed scatter indicates an intrinsic variation in the ICL fraction. On the other hand, there is a weak relationship between the fraction of ICL and the fraction of early-type galaxies in the host halo, where a larger fraction of ICL is found in groups and clusters of galaxies dominated by earlier morphological types, indicating a connection between the ICL and the dynamical state of the host system.

Key words. galaxies: evolution – galaxies: photometry – galaxies: groups: general – galaxies: clusters: general – galaxies: interactions – galaxies: clusters: intracluster medium

1. Introduction

Since it was proposed and subsequently observed by Zwicky (1937, 1951, 1952, 1957) in the Coma cluster, we know that there is an additional component in the light distribution of galaxy clusters, namely, intra-cluster light (ICL). The ICL is made of baryons (stars and globular clusters) that are gravitationally unbound to any specific galaxy in the cluster, observed as a diffuse and very faint emission ($\mu_V > 26.5$ mag arcsec^{-2}, Mihos et al. 2005), extending out to several hundred of kpc from the cluster centre (see Montes 2019 and references therein). According to the ΛCDM paradigm, the ICL is the product of the gravitational interactions (accretion and merging) involved in the formation of the most massive galaxies at the centre of groups and clusters, known as the brightest group (BGG) or cluster (BCG) galaxy. Therefore, the ICL is usually more concentrated around the BCG (or BGG), as confirmed by observations (e.g., Mihos et al. 2005; Arnaboldi et al. 2012). Several formation channels have been proposed for the build-up of the ICL, which may all happen in the same environment: (i) tidal stripping of satellites in the potential well of the BCG (Rudick et al. 2009; Contini et al. 2014, 2019), (ii) disruption of dwarf galaxy members (Purcell et al. 2007), (iii) major mergers with the BCG or BGG (Murante et al. 2007; Conroy et al. 2007), (iv) pre-processing in groups (Mihos et al. 2005; Rudick et al. 2006), or (v) from unbound stars formed in situ (Puchwein et al. 2010). The low-surface-brightness (LSB) features resulting from these processes (e.g., shells, tidal tails, stellar streams) also contribute (i.e., by a few percent) to the total amount of ICL (e.g., Gonzalez et al. 2013; Presotto et al. 2014; Contini et al. 2018). Hence, the ICL represents the fossil record of the mass assembly in galaxies. As a consequence, the physical properties of the ICL (e.g., total luminosity, colors, stellar populations) allow us to constrain the formation channels for this component, including the look-back time and the dynamical state of the system (see Contini 2021; Montes 2022 and references therein). Simulations agree that the bulk of the ICL forms in the redshift range of $0 \leq z \leq 1$, with the total amount of ICL increasing up by ∼20% to $z = 0$. In this context, one of the key parameters is the fraction of ICL, $f_{\rm ICL}$ (Sect. 3.1). From

a theoretical perspective, more evolved clusters are expected to have larger values of $f_{\rm ICL}$, since galaxies in the dense environment of galaxy clusters are expected to have experienced more gravitational interactions (e.g., Murante et al. 2007; Rudick et al. 2011; Martel et al. 2012; Contini et al. 2014). One way to constrain the physical processes that form the ICL is to see how $f_{\rm ICL}$ correlates with the virial mass ($M_{\rm vir}$) of the host environment. Theoretical predictions report contradictory results. According to several works (Sommer-Larsen 2006; Monaco et al. 2006; Henriques & Thomas 2010; Rudick et al. 2011; Contini et al. 2014), in the halo mass range of $M_{\rm vir} \simeq 10^{13}-10^{15}\,M_{\odot}$, $f_{\rm ICL}$ spans from 20% to 40%, without showing any trend with $M_{\rm vir}$. Conversely, increasing values of $f_{\rm ICL}$, from 20% up to 40%, with increasing $M_{\rm vir}$ have been predicted in several simulations (Lin & Mohr 2004; Murante et al. 2007; Purcell et al. 2007; Pillepich et al. 2018; Henden et al. 2019; Ahad et al. 2023). An opposite trend was suggested by Cui et al. (2013), whereby a decreasing $f_{\rm ICL}$ (from ∼50% to ∼40%) with increasing $M_{\rm vir}$ is predicted. Due to its low-surface-brightness nature, the detection and study of the ICL is a challenging task, requiring very deep images over large areas around the center of the clusters or groups. So far, the few available measurements of $f_{\rm ICL}$ have prevented any conclusion to be drawn on the correlation with $M_{\rm vir}$ (see Contini 2021; Montes 2022 as reviews, and references therein). In the Local Universe ($z \leq 0.05$), $f_{\rm ICL}$ spans a wide range of values (from 10% up to ∼50%) for any $M_{\rm vir}$; therefore, it seems that the two quantities are not correlated (Ragusa et al. 2021, 2022; Montes 2022). A similar result is obtained for ICL measurements at higher redshift ($0.2 \leq z \leq 0.35$, e.g., Sampaio-Santos et al. 2021; Martínez-Lombilla et al. 2023). On the other hand, it seems that a mild trend is observed between $f_{\rm ICL}$ and the fraction of the early type galaxies ($f_{\rm ETGs} = {\rm ETGs}/[{\rm ETGs} + {\rm LTGs}]$), namely: the fraction of ICL is larger in those environments dominated by early-type galaxies (Da Rocha et al. 2008; Ragusa et al. 2021, 2022). Even considering the few data points available, Iodice et al. (2020) found that the $f_{\rm ICL}$ seems to increase with decreasing amount of neutral hydrogen (HI) in the host system, another tracer of the evolutionary state of the system (e.g., Kilborn et al. 2009). However, these results need to be confirmed with larger data sets. In particular, since the ICL content can be estimated using several methods (see the review by Montes 2022) and, in addition, it depends on the depth of the data and on the adopted data analysis, the main requirements needed to address the dependencies of the $f_{\rm ICL}$ with $M_{\rm vir}$ and the evolutionary state of the environments are a homogeneous and statistically significant sample of groups and clusters of galaxies, spanning the whole halo mass range covered by the theoretical predictions.

In this Letter, we revisit the relationships between $f_{\rm ICL}$ vs. $M_{\rm vir}$ and $f_{\rm ICL}$ vs. $f_{\rm ETGs}$ based on a sample of 22 groups and clusters, covering $10^{12.5} \leq M_{\rm vir} \leq 10^{14.5}\,M_{\odot}$ in the local Universe (i.e., $z \leq 0.05$), from the VST Early-type GAlaxy Survey (VEGAS, Capaccioli et al. 2015; Iodice et al. 2021). The images were all acquired with the same observational setup, with comparable depths (within ∼0.5 mag) and all analysed using the same methodology. This allows us to overcome many of the limitations mentioned above and provide more robust results on the connection between the ICL fraction and the properties of the host environment. The Letter is organized as follows. In Sect. 2, we present the VEGAS observations and the data reduction strategies used for this work. In Sect. 3 we describe the data analysis we performed. Finally, in Sect. 4 we illustrate our results and make a comparison with theoretical predictions. Overall, we assume $H_0 = 73\,{\rm km\,s^{-1}\,Mpc^{-1}}$, $\Omega_{\rm M} = 0.3$, and $\Omega_{\Lambda} = 0.7$.

2. Deep images from VEGAS: Observations and data reduction

The VEGAS sample presented in this Letter is made up of 22 targets in total, five of which have already been subject of previous works, covering the core of groups and clusters of galaxies in the low-redshift regime ($z \leq 0.05$). These 17 new targets reported here are listed in Table 1. VEGAS is a multi-band, deep imaging survey (Iodice et al. 2021), based on the observations acquired with the ESO VLT Survey Telescope (VST), a 2.6 meter optical telescope located at Cerro Paranal, Chile (Schipani et al. 2012). The VST is equipped with the wide field camera, OmegaCAM, with a field of view of $1^{\circ} \times 1^{\circ}$ and a resolution of $0.21\,{\rm arcsec\,pixel^{-1}}$. The data presented in this work were acquired in different visitor or service mode runs, in dark time and in clear conditions. The data reduction was performed using the dedicated AstroWISE (for more details see McFarland et al. 2013; Venhola et al. 2017) or VST-Tube (Capaccioli et al. 2015) pipelines, both capable of providing equivalent results. A detailed description of the observing setup and data reduction for the VEGAS images has been presented in several papers (e.g., Capaccioli et al. 2015; Iodice et al. 2016, 2020; Spavone et al. 2017; Cattapan et al. 2019; Ragusa et al. 2021), to which we refer for a comprehensive description and, in particular, for the adopted tools and methods for the background removal, which is fundamental in such LSB studies. All targets in our sample are observed in the g and r filters, some of them also have images acquired in the u and/or i bands. In this Letter, we focus on the ICL estimates derived in the g band, which is the most efficient OmegaCAM filter (Kuijken 2011). All g-band images have a total integration time of ∼2.5 h. The surface brightness depth at 5σ over an area of the average seeing of FWHM ∼ 1 arcsec is $\mu_g \sim 29-30\,{\rm mag\,arcsec^{-2}}$, which is about six magnitudes fainter than the surface brightness of the night sky in the g band at ESO-Paranal (∼22.5 mag arcsec^{-2}, Desai et al. 2012). In Fig. 1, we show the resulting sky-subtracted color composite VST image obtained for the NGC 3640 group. This image reveals the plethora of shells and tidal tails detected around the BGG (NGC 3640) and shows how the data acquisition and reduction perform well enough to unveil the LSB features in the galaxy outskirts and intra-group space.

3. Data analysis

The data analysis used here was aimed at estimating the ICL for all the targets in our sample, based on the well-tested surface photometry of the galaxies, which is described in detail in our recent paper (Ragusa et al. 2021). The two main preliminary steps are: (i) removal of the bright stars in the field and (ii) estimation of the limiting radius of the surface photometry. In short, to account for the scattered light from the bright stars in the field that might affect the estimate of the ICL, these are modelled and subtracted from the original image. During this step, the core of the group (or cluster) is also masked out to ∼10–20 $R_{\rm eff}$ of the BCGs to avoid accounting for part of the ICL in the scattered light. On the star-subtracted images, we estimated the limiting radius of the photometry ($R_{\rm lim}$, hereafter). This corresponds to the outermost radius with respect to the center of the target, where the galaxy's light blends into the residual background fluctuations. This task is performed by fitting the light

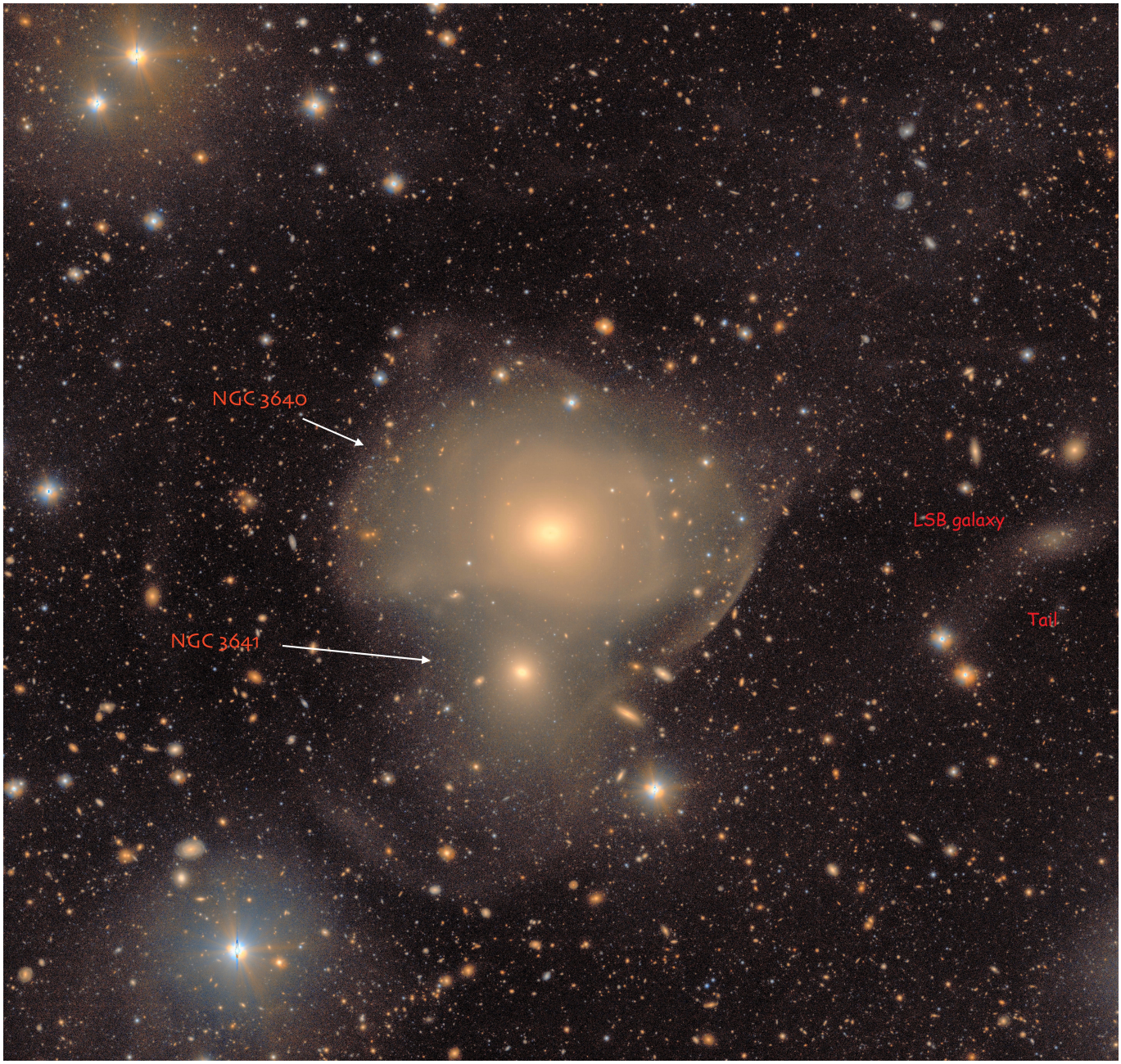

Fig. 1. Color composite (*gri*) VST image of the NGC 3640 group. The image size is ∼20 × 20 arcmin. North is up and east is to the left. The brightest group members are labelled in red on the image. The image is chosen as a target example for the VEGAS sample, given how clearly LSB features ($\mu_g > 29$ mag arcsec^{-2}) such as shells and tidal tails are evident in the outskirts of the central galaxy. Moreover, on the west side of NGC 3640, a LBS galaxy is also detected, with a very faint tail towards the BGG (Mirabile et al., in prep.). For this target, the fraction of IGL plus diffuse stellar envelope, estimated in Sect. 3 as ∼8%, comes mainly in the form of shells and tidal tails around the BGG.

distribution in the frame in circular annuli, centred on the BCG (or BGG).

3.1. Measuring the ICL

According to the two-phase formation scenario of galaxy formation, the inner and brighter part of the BCG is formed first, with a surface brightness profile that is well reproduced by a Sérsic law. During the accretion phase, the bounded stellar envelope and unbounded ICL are built around the BCG. Given their similar accreted origin, based on photometry alone, it is not possible to unambiguously separate the ICL from the stellar envelope, since the transition between these two components occurs very smoothly and sometimes it is completely indistinguishable, as both components show a similar surface-brightness profile. For this reason, the $f_{\rm ICL}$ is commonly defined as the total contribution from the diffuse and unbounded intra-cluster baryons plus the stellar envelope around galaxies. There are different photometric methods in the literature used to separate the ICL from the BCG (see Montes 2022, as review). One of the proposed and more reliable methods is based on the 1D or 2D multi-component decomposition of the BCG light distribution, where the brightest regions of the BCG can be distinguished from the stellar envelope and ICL (e.g., Gonzalez et al. 2007; Kravtsov et al. 2018;

Table 1. New unpublished VEGAS sample of groups and clusters and ICL estimates.

Target	Environ.	RA [J2000]	Dec [J2000]	D [Mpc]	$m_{\mathrm{ICL},g}$ [mag]	$L_{\mathrm{ICL},g}$ [$10^{10}\,L_{\odot}$]	R_{vir} [Mpc]	M_{vir} [$10^{13}\,M_{\odot}$]	$L_{\mathrm{ICL},g}/L_{\mathrm{tot},g}$	f_{ETGs}
(1)	(2)	(3)	(4)	(5)	(6)	(7)	(8)	(9)	(10)	(11)
Antlia	cluster	10:30:00.7	−35:19:31.7	40.0	10.27 ± 0.07	18.80 ± 1.20	1.28	26.3	0.32± 0.03	0.76
HCG 86	compact gr.	19:52:08.8	−30:49:32.7	82.0	13.90± 0.10	2.80 ± 0.30	0.41	0.85	0.16 ± 0.03	1.00
NGC 596/584	group	01:32:12.1	−06:56:54.6	27.0	13.21± 0.08	0.58 ± 0.04	0.50	1.55	0.05± 0.01	0.40
NGC 1453	group	03:46:27.3	−03:58:07.6	55.5	14.00 ± 0.10	1.20 ± 0.10	0.86	4.00	0.05± 0.01	0.50
NGC 1553	group	04:16:10.5	−55:46:48.5	17.3	10.86 ± 0.09	2.70 ± 0.20	0.80	5.89	0.17± 0.02	0.75
NGC 3100	group	10:00:40.8	−31:39:52.4	36.0	13.70± 0.06	0.66± 0.04	0.52	1.78	0.05 ± 0.01	0.33
NGC 3258	Antlia sub-gr.	10:28:53.6	−35:36:19.9	41.0	11.70± 0.07	5.00± 0.30	0.46	1.17	0.27± 0.03	0.76
NGC 3268	Antlia sub-gr.	10:30:00.7	−35:19:31.7	40.0	10.60 ± 0.07	13.80 ± 0.90	0.90	8.99	0.34 ± 0.03	0.70
NGC 3379	group	10:47:49.6	+12:34:53.9	10.2	10.72 ± 0.08	1.22± 0.09	0.47	1.26	0.17± 0.02	1.00
NGC 3640	group	11:21:06.9	+03:14:05.4	18.0	13.20± 0.10	0.30 ± 0.03	0.40	0.79	0.08± 0.01	1.00
NGC 3923	group	11:51:01.7	−28:48:21.7	23.0	10.01 ± 0.05	7.80± 0.40	0.60	2.69	0.35 ± 0.03	0.67
NGC 4365	Virgo W' Cloud	12:24:28.3	+07:19:03.6	21.3	10.79 ± 0.08	3.30± 0.20	0.32	0.40	0.18± 0.02	0.40
NGC 4636	Virgo sub-gr.	12:42:49.9	+02:41:16.0	20.0	12.01 ± 0.08	0.95± 0.07	0.63	3.02	0.07± 0.02	0.33
NGC 4697	Virgo sub-gr.	12:48:35.9	−05:48:02.7	18.0	11.00 ± 0.05	1.95± 0.09	1.29	26.9	0.20 ± 0.02	1.00
NGC 5044	group	13:15:24.0	−16:23:07.9	32.0	10.84 ± 0.07	7.20 ± 0.50	0.80	6.31	0.22± 0.03	0.71
NGC 5846	group	15:06:29.3	+01:36.20.3	25.0	10.17 ± 0.06	8.10± 0.40	1.10	16.6	0.28± 0.03	0.83
NGC 6868	group	20:09:54.1	−48:22:46.4	41.0	11.36 ± 0.07	7.20± 0.50	0.60	2.69	0.30± 0.03	0.67

Notes. In Col. 1: the name of the BGG-BCG and Col. 2: the environment in which the target lies. Columns 3 and 4: the celestial coordinates of the group-cluster center. Column 5: the distance of the BCG. Columns 6 and 7: the magnitude and luminosity of the ICL component, in the g band, respectively (from our work). Columns 8 and 9: the virial radius and virial mass inside the virial radius, respectively. Column 10: the fraction of the ICL component with respect to the total luminosity of the group-cluster in the g band. Column 11: the fraction of the ETGs with respect to the total number of galaxies, taking into account the brighter galaxies studied in each system. All the magnitudes listed in the table are corrected for Galactic extinction using the extinction coefficients provided by Schlafly & Finkbeiner (2011). To compute the $L_{\odot,g}$, we use the prescriptions from Blanton et al. (2003), with $M_{\odot,g} = 5.45$ mag. For the M_{vir} (R_{vir}), we assumed the following values: NGC 3923, NGC 4636, and NGC 5044 from Brough et al. (2006); NGC 6868, NGC 596/584, NGC 3640, NGC 4697, and NGC 5846 from Gourgoulhon et al. (1992); NGC 4365 from Samurović (2014); HCG 86 from Coziol et al. (2004); NGC 3379 from Karachentsev et al. (2015); NGC 3258, NGC 3268, and the Antlia cluster from Calderón et al. (2020); NGC 3100 from (Tempel et al. 2016); and NGC 1453 from (Pandya et al. 2017). To estimate all the distances of this work, we used the heliocentric radial velocity, given by NED (NASA IPAC Extragalactic Database) and $H_0 = 73\,\mathrm{km\,s^{-1}\,Mpc^{-1}}$ (Riess et al. 2018).

Zhang et al. 2019; Kluge et al. 2020; Montes et al. 2021). In detail, by fitting the light distribution of the BCG with empirical laws, the transition region between the gravitationally bound and brightest regions of the BCG and the stellar envelope, plus the ICL, is constrained. As commented earlier in this work, due to the difficulty separating between the BCG, the bounded stellar halo, and the unbounded ICL, the total amount of ICL reported here includes the contribution from the stellar envelope and the unbound diffuse light. Therefore, the total amount of ICL must be considered an upper limit.

We have adopted this method to study the stellar halos in BCGs and to estimate the contribution of ICL from VEGAS images. It is described and applied in several published papers (Cattapan et al. 2019; Iodice et al. 2020; Spavone et al. 2020; Raj et al. 2020; Ragusa et al. 2021, 2022). Below, we summarize the main steps that lead to the estimate of f_{ICL} in the g band.

One-dimensional multi-component decomposition of the BCGs. We performed the 1D multi-component decomposition of the BCG' azimuthally-averaged surface brightness profiles, adopting the procedure introduced by Spavone et al. (2017). This provides the estimate of the transition radius (R_{tr}, hereafter) in each galaxy. Then, R_{tr} is the distance from the galaxy centre where the contribution from the galaxy outskirts (i.e., stellar envelope plus diffuse light) starts to dominate the total light distribution. Thus, based on the isophote fit, we derived a 2D model of the BCG light distribution out to R_{tr} and subtracted it from the parent image.

Residual images. On the residual image obtained in the previous step, using the same multi-component fitting approach, we have also modelled the light from all the other galaxy members (out to R_{lim}), including those objects that do not show a prominent contribution of diffuse light in the outskirts. All the 2D models have been subtracted from the parent image. The resulting residual image traces the spatial distribution of the stellar envelopes, plus the ICL in the group or cluster, and this is used to compute its total luminosity ($L_{\mathrm{ICL},g}$). The value of $L_{\mathrm{ICL},g}$ for all targets in our sample is reported in Table 1.

Estimate of the ICL fraction. The f_{ICL} is defined as the ratios $L_{\mathrm{ICL},g}/L_{\mathrm{tot},g}$, where $L_{\mathrm{ICL},g}$ is the total luminosity of the ICL and $L_{\mathrm{tot},g}$ is the total luminosity of the group or cluster in the g band, including the ICL. The value of $L_{\mathrm{tot},g}$ is obtained by summing up the total luminosity derived for all cluster (or group) members plus $L_{\mathrm{ICL},g}$. All the above values for the targets in our sample are listed in Table 1. The error estimate on $L_{\mathrm{ICL},g}$ and $L_{\mathrm{tot},g}$ takes into account the uncertainties on the photometric calibration, the rms in the background fluctuations, and the Poissonian error assumed for the total integrated flux[1].

The surface photometry for all galaxies in all targets of our sample (i.e., surface brightness profiles, colors, integrated magnitudes, and total luminosity), derived by the isophote fitting, will be presented and discussed in a forthcoming paper (Ragusa et al., in prep.). In this Letter, we focus on the main outcome of this analysis: the estimate of the ICL for such a large and homogeneous sample of groups and clusters of galaxies.

[1] The error on the total magnitude is computed as follow: $\mathrm{err_{mag}} = \sqrt{\{2.5/[\mathrm{flux}\times\ln(10)]\}^2\times[(\mathrm{err_{flux}}+\mathrm{err_{sky}})^2]+\mathrm{err}_{zp}^2}$, where $\mathrm{err_{sky}}$ is the rms on the sky background, err_{zp} is the error on the photometric calibration, and $\mathrm{err_{flux}} = \sqrt{\mathrm{flux}/N-1}$ is the poissonian error on the integrated flux from a total number of N pixels used in the isophote fit.

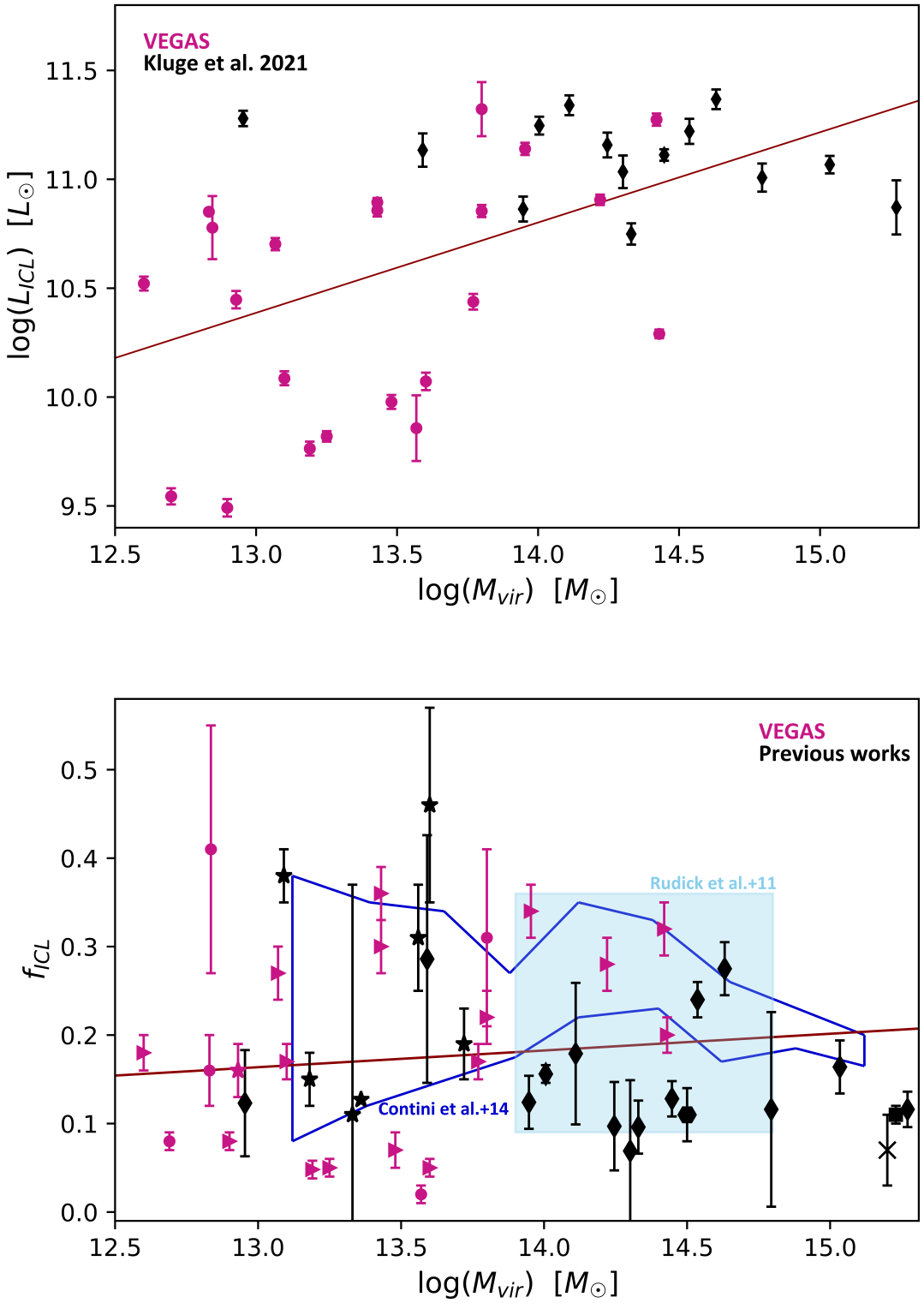

Fig. 2. Relationships between ICL amount as a function of $M_{\rm vir}$. *Top panel*: luminosity of the ICL component as a function of the $M_{\rm vir}$. The best fit for the linear correlation is shown by the dark-red solid line. The best fit equation is $\log(L_{\rm ICL}) = (0.41 \pm 0.11) * \log(M_{\rm vir}) - (5 \pm 1.5)$, with $R^2 = 28\%$ and p-value = 0. *Lower panel*: ICL fraction ($f_{\rm ICL}$) vs. $M_{\rm vir}$ obtained for the VEGAS targets (magenta symbols), compared with the values of $f_{\rm ICL}$ available in the literature, for targets at $z \leq 0.05$ (black points). These are the compact groups from Da Rocha & Mendes de Oliveira (2005), Da Rocha et al. (2008), Pildis et al. (1995), Poliakov et al. (2021) Ragusa et al. (2021, stars), the Coma cluster (Jiménez-Teja et al. 2019, octagon), the Virgo cluster (Mihos et al. 2017, cross) and the Abell 85 cluster (Montes et al. 2021, square). The clusters of galaxies from Kluge et al. (2021) are also included in this plot (diamonds). The virial masses for the cluster in the latter sample are from Kluge (2020), when available. For systems with no estimation of the viral mass, we used the velocity dispersion of the member galaxies reported in Kluge (2020) to estimate it following Munari et al. (2013). The solid line indicates the best fit for the linear correlation. The best fit equation is $f_{\rm ICL} = (0.02 \pm 0.02) * \log(M_{\rm vir}) - (0.07 \pm 0.34)$, with $R^2 = 1.6$ % and p-value = 0.47. The theoretical prediction obtained by Contini et al. (2014; blue contours) and Rudick et al. (2011; light blue area) are included for comparison.

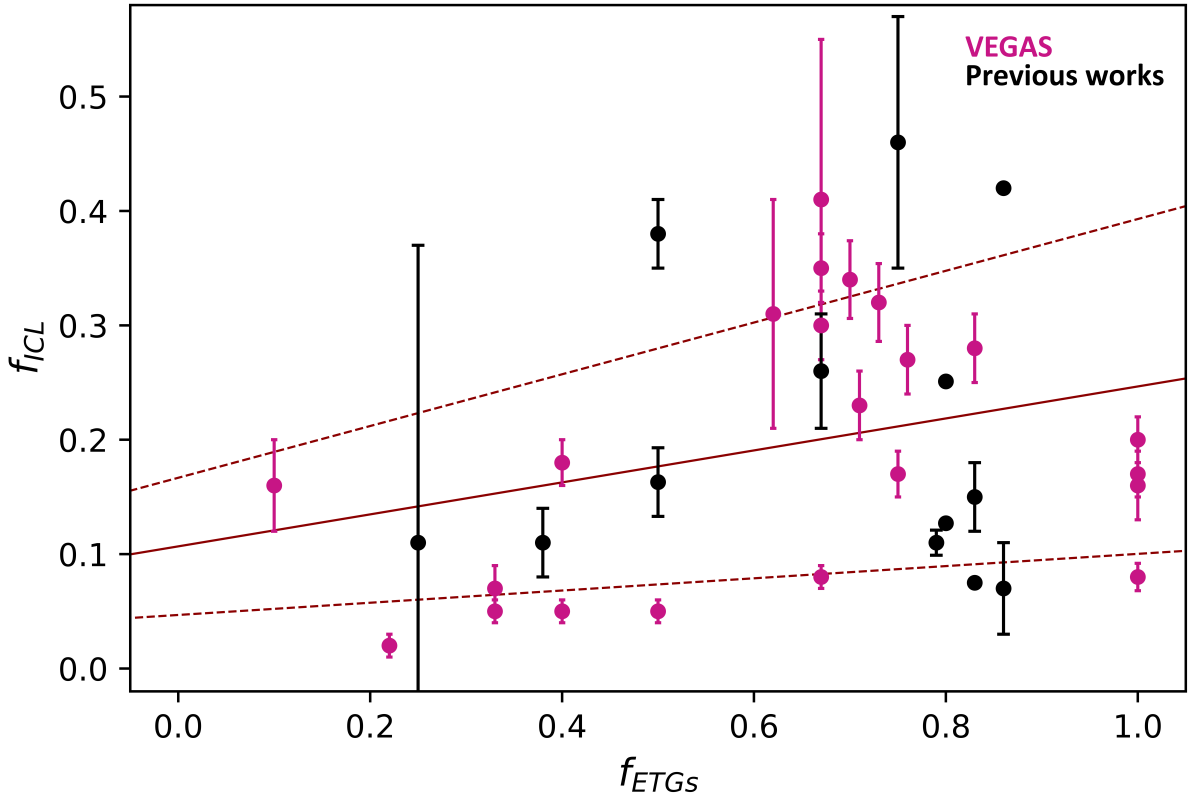

Fig. 3. ICL fraction ($f_{\rm ICL}$) as a function of the $f_{\rm ETGs}$. The values for the ICL obtained from VEGAS are marked in magenta and the other estimates for groups and clusters of galaxies available in the literature in black (same references as in Fig. 2). A weak trend exists between the two quantities, as indicated by the dark-red solid line, which reflects the best fit for the linear correlation. The dashed red lines mark the 1σ significance range of that correlation. The best-fit equation is $f_{\rm ICL} = (0.14 \pm 0.08) * f_{\rm ETGs} - (0.11 \pm 0.06)$, with $R^2 \sim 10\%$ and p-value = 0.12.

4. Discussion

The main goal of this Letter is to revisit the relationship between the ICL fraction with (i) the halo mass of the environment ($M_{\rm vir}$), as shown in Fig. 2, and (ii) with the fraction of the evolved galaxy members (ETGs), as shown in Fig. 3. To date, both of these relationships have remained uncertain, and theoretical predictions have not provided any constraints (see Sect. 1). As far as ICL estimates are concerned, in the halo mass range $10^{12.5} \leq M_{\rm vir} \leq 10^{15.5}\,M_{\odot}$, with the new sample presented in this work, we significantly expanded on the store of statistics for the study of both relationships, doubling the previous literature estimates based on a homogeneous sample (see Sect. 3). Therefore, all possible biases in the results due to observational setup and/or methodology are minimized.

4.1. ICL versus $M_{\rm vir}$

In Fig. 2, we plot $L_{\rm ICL}$ (upper panel) and $f_{\rm ICL}$ (lower panel) vs. $M_{\rm vir}$ of the environment, for a sample of 46 systems at $z \leq 0.05$. The VEGAS sample accounts for 22 targets. The remaining 24 targets come from the literature, where $f_{\rm ICL}$ was obtained with similar methods used in this work, as well as in the optical wavelength bands, to avoid introducing any bias in the relationship. As expected, a mild trend is found for $L_{\rm ICL}$ vs. $M_{\rm vir}$ (see Fig. 2, upper panel), since more satellite galaxies lead to the formation of a greater volume of the ICL (e.g., Sampaio-Santos et al. 2021; Kluge et al. 2021). Conversely, the trend disappears for $f_{\rm ICL}$ vs. $M_{\rm vir}$ (see Fig. 2, lower panel). In particular, we found that a large $f_{\rm ICL}$ (~30–40%) can be present in both loose and less massive groups of galaxies, such as NGC 5018 ($M_{\rm vir} < 10^{13}\,M_{\odot}$), and in rich and massive clusters of galaxies, such as the Antlia cluster ($M_{\rm vir} \sim 10^{14}\,M_{\odot}$). Similarly, a small $f_{\rm ICL}$ (0–15%) has been detected in both compact and less massive groups, ($10^{13}\,M_{\odot} < M_{\rm vir} < 10^{13.5}\,M_{\odot}$), as well as in very rich and massive clusters, such as Abell 85 and Coma ($10^{15}\,M_{\odot} < M_{\rm vir} < 10^{15.5}\,M_{\odot}$). Based on this plot and in agreement with previous results by Ragusa et al. (2021, 2022) and Montes (2022) on a smaller sample of data, a large scatter is observed for $f_{\rm ICL}$ vs. $M_{\rm vir}$. The two quantities do not show any strong correlation, as confirmed by the linear regression best fit to the sample. Since most of the data in Fig. 2 come from a data set with the same depth and methodology. Thus, it is reasonable to conclude that the observed scatter in this plot is intrinsic, and it cannot be due to inconsistencies in the data acquisition and analysis. As addressed in Sect. 1, theoretical predictions provide different and sometimes contradictory results on the relationship between $f_{\rm ICL}$ and $M_{\rm vir}$. The large range of estimates now made available from this work allow us to provide stringent constraints on the most reliable scenario connecting the two physical quantities. In the lower panel of Fig. 2, we superpose the theoretical predictions by Contini et al. (2014) and Rudick et al. (2011). Neither works predict a significant trend between the fraction of ICL and the halo mass of the host environment, which is in agreement with the new observations. In particular, in their mass ranges and resolutions, they found that $9\% \leq f_{\rm ICL} \leq 40\%$, which is consistent with the measured range presented here. The absence of a strong physical connection between the fraction of ICL and the halo mass of the host environment found here would suggest that the formation mechanisms of the ICL do not depend on the potential

well where it is located and they are equivalently efficient at the scale of both groups and clusters (see also Cañas & Lagos 2020). In particular, the bulk of the ICL formation might happen in groups of galaxies that subsequently join the cluster potential and a smaller fraction of ICL would be formed later in the cluster environment. In support of this argument, the two sub-groups of the Antlia cluster presented in this Letter have comparable values of $f_{\rm ICL}$ to that estimated for the whole cluster. This would point toward a different efficiency of the several formation channels proposed for the build-up of the ICL and, in particular, towards the pre-processing in groups as the main channel for the build-up of the bulk of the ICL.

4.2. ICL fraction versus $f_{\rm ETGs}$

In Fig. 3, we show $f_{\rm ICL}$ as a function of the ratio between early-type and the total number of bright galaxies ($f_{\rm ETGs}$, with $M_B \leq 16$) in the host environment for the VEGAS sample and for those targets in the literature for which an estimate is available. As already pointed out by Ragusa et al. (2021), this larger sample hints that systems with a higher number of ETGs show a larger fraction of ICL. Fitting all the points with a linear regression, we find a weak trend between $f_{\rm ICL}$ and $f_{\rm ETGs}$. However, within 1σ from the best fit, the scatter is also quite large. The $f_{\rm ICL}$ ranging from 5% up to 40% across the whole range of $f_{\rm ETGs}$. Similarly, we found that groups or clusters of galaxies with a comparable fraction of ICL, in the range between 5 and 15%, show very different $f_{\rm ETGs}$, from 0 to 1. The weak trend with the $f_{\rm ETGs}$ found here supports the idea that the fraction of ICL is connected with the efficiency of the several formation channels, namely, gravitational interactions, such as tidal stripping and merging, which are more frequent in environments that are more dynamically evolved – namely, those that show a larger $f_{\rm ETGs}$ ratio.

5. Conclusions

In this Letter, we present new estimates of the intra-cluster light fraction, based on deep images from VEGAS, for a homogeneous and large sample (22 targets) of groups and clusters of galaxies, in the halo mass range $10^{12.5} \leq M_{\rm vir} \leq 10^{14.5}\,M_{\odot}$, for $z \leq 0.05$. We have found that the $f_{\rm ICL}$ ranges from ∼5% up to ∼50%. Such values are consistent with the predicted $f_{\rm ICL}$ from several theoretical studies. We have investigated the relation between $f_{\rm ICL}$ and the halo mass of the target as well as its fraction of early-type galaxies, by combining our targets with estimates for additional 24 targets, available from previously published works. The large sample allows us to confirm that although it would be expected in those systems with more satellite galaxies for $L_{\rm ICL}$ to increase with $M_{\rm vir}$, in fact, $f_{\rm ICL}$ does not depend on the $M_{\rm vir}$ of the host environment. This finding is in agreement with predictions from Contini et al. (2014) and Rudick et al. (2011). This also has fundamental implications for the assembly history of groups and clusters. The $f_{\rm ICL}$ depends on the efficiency of the formation mechanisms of this diffuse light being greater in those systems with a large number of more evolved galaxies, as also suggested from the mild relation between the $f_{\rm ICL}$ and $f_{\rm ETGs}$ found in this work. The lack of a strong correlation between $f_{\rm ICL}$ and $M_{\rm vir}$ leads us to conclude that the bulk of the ICL is assembled at the group scale and then incorporated into the clusters during the group infall. It is worth noting that in /the $f_{\rm ICL}$ vs. $M_{\rm vir}$ plane, we cover the low $M_{\rm vir}$ range ($10^{12.5} \leq M_{\rm vir} \leq 10^{13.5}\,M_{\odot}$) well, which had been poorly covered in previous works. The lack of more ICL estimates for the most massive clusters of galaxies ($10^{14.5} \leq M_{\rm vir} \leq 10^{15.5}\,M_{\odot}$) for $z \leq 0.05$ is mainly due to the lack of deep images covering the large area needed for such a systems, which require extended mosaics with the available wide-field telescopes for surveys. The upcoming observing facilities, aimed at covering large portions of the sky down to the LSB regime (such as the ten-year Legacy Survey of Space and Time, which will take place at the *Vera C. Rubin* Observatory, e.g., Montes & Trujillo 2019; Brough et al. 2020), will be able to provide also accurate ICL estimates in this halo mass range.

Acknowledgements. This study benefits from the observations gathered at the European Southern Observatory (ESO) La Silla Paranal Observatory within the VST Guaranteed Time Observations, Programme IDs: 090.B-0414(B), 090.B-0414(D), 091.B-0614(A), 091.B-0614(B), 092.B-0623(B), 094.B- 0496(A), 094.B-0496(B), 094.B-0496(D), 095.B-0779(A), 096.B-0582(B), 097.B-0806(A), 0101.A-0166(B), 103.A-0181(A), 0104.A-0072(B). Authors acknowledge financial support from the VST project (P.I. P. Schipani) and from the INAF-OACN. Authors are very grateful to M. Kluge for providing the ICL estimates from the data set he studied. MM acknowledges the Project PCI2021-122072-2B, financed by MICIN/AEI/10.13039/501100011033, and the European Union "NextGenerationEU"/RTRP. Authors wish also to thank the anonymous referee for all suggestions, which helped to improve this manuscript.

References

Ahad, S. L., Bahé, Y. M., & Hoekstra, H. 2023, MNRAS, 518, 3685
Arnaboldi, M., Ventimiglia, G., Iodice, E., Gerhard, O., & Coccato, L. 2012, A&A, 545, A37
Blanton, M. R., Hogg, D. W., Bahcall, N. A., et al. 2003, ApJ, 592, 819
Brough, S., Forbes, D. A., Kilborn, V. A., & Couch, W. 2006, MNRAS, 370, 1223
Brough, S., Collins, C., Demarco, R., et al. 2020, ArXiv e-prints [arXiv:2001.11067]
Cañas, R., Lagos, C., d. P., Elahi, P. J., , et al. 2020, MNRAS, 494, 4314
Calderón, J. P., Bassino, L. P., Cellone, S. A., Gómez, M., & Caso, J. P. 2020, MNRAS, 497, 1791
Capaccioli, M., Spavone, M., Grado, A., et al. 2015, A&A, 581, A10
Cattapan, A., Spavone, M., Iodice, E., et al. 2019, ApJ, 874, 130
Conroy, C., Wechsler, R. H., & Kravtsov, A. V. 2007, ApJ, 668, 826
Contini, E. 2021, Galaxies, 9, 60
Contini, E., Yi, S. K., & Kang, X. 2018, MNRAS, 479, 932
Contini, E., Yi, S. K., & Kang, X. 2019, ApJ, 871, 24
Contini, E., De Lucia, G., Villalobos, Á., & Borgani, S. 2014, MNRAS, 437, 3787
Coziol, R., Brinks, E., & Bravo-Alfaro, H. 2004, AJ, 128, 68
Cui, W., Murante, G., Monaco, P., et al. 2013, MNRAS, 437, 816
Da Rocha, C., & Mendes de Oliveira, C. 2005, MNRAS, 364, 1069
Da Rocha, C., Ziegler, B. L., & Mendes de Oliveira, C. 2008, MNRAS, 388, 1433
Desai, S., Armstrong, R., Mohr, J. J., et al. 2012, ApJ, 757, 83
Gonzalez, A. H., Zaritsky, D., & Zabludoff, A. I. 2007, ApJ, 666, 147
Gonzalez, A. H., Sivanandam, S., Zabludoff, A. I., & Zaritsky, D. 2013, ApJ, 778, 14
Gourgoulhon, E., Chamaraux, P., & Fouque, P. 1992, A&A, 255, 69
Henden, N. A., Puchwein, E., & Sijacki, D. 2019, MNRAS, accepted
Henriques, B. M. B., & Thomas, P. A. 2010, MNRAS, 403, 768
Iodice, E., Capaccioli, M., Grado, A., et al. 2016, ApJ, 820, 42
Iodice, E., Spavone, M., Cattapan, A., et al. 2020, A&A, 635, A3
Iodice, E., Spavone, M., Capaccioli, M., et al. 2021, The Messenger, 183, 25
Jiménez-Teja, Y., Dupke, R. A., Lopes de Oliveira, R., et al. 2019, A&A, 622, A183
Karachentsev, I. D., Nasonova, O. G., & Karachentseva, V. E. 2015, Astrophys. Bull., 70, 1
Kilborn, V. A., Forbes, D. A., Barnes, D. G., et al. 2009, MNRAS, 400, 1962
Kluge, M. 2020, PhD Thesis, Ludwig-Maximilians University of Munich, Germany
Kluge, M., Neureiter, B., Riffeser, A., et al. 2020, ApJS, 247, 43
Kluge, M., Bender, R., Riffeser, A., et al. 2021, ApJs, 252, 27
Kravtsov, A. V., Vikhlinin, A. A., & Meshcheryakov, A. V. 2018, Astron. Lett., 44, 8
Kuijken, K. 2011, The Messenger, 146, 8
Lin, Y.-T., & Mohr, J. J. 2004, ApJ, 617, 879
Martel, H., Barai, P., & Brito, W. 2012, ApJ, 757, 48

Martínez-Lombilla, C., Brough, S., Montes, M., et al. 2023, MNRAS, 518, 1195
McFarland, J. P., Verdoes-Kleijn, G., Sikkema, G., et al. 2013, Exp. Astron., 35, 45
Mihos, J. C., Harding, P., Feldmeier, J., & Morrison, H. 2005, ApJ, 631, L41
Mihos, J. C., Harding, P., Feldmeier, J. J., et al. 2017, ApJ, 834, 16
Monaco, P., Murante, G., Borgani, S., & Fontanot, F. 2006, ApJ, 652, L89
Montes, M. 2019, ArXiv e-prints [arXiv:1912.01616]
Montes, M. 2022, Nat. Astron., 6, 308
Montes, M., & Trujillo, I. 2019, MNRAS, 482, 2838
Montes, M., Brough, S., Owers, M. S., & Santucci, G. 2021, ApJ, 910, 45
Munari, E., Biviano, A., Borgani, S., Murante, G., & Fabjan, D. 2013, MNRAS, 430, 2638
Murante, G., Giovalli, M., Gerhard, O., et al. 2007, MNRAS, 377, 2
Pandya, V., Greene, J. E., Ma, C.-P., et al. 2017, ApJ, 837, 40
Pildis, R. A., Bregman, J. N., & Schombert, J. M. 1995, AJ, 110, 1498
Pillepich, A., Nelson, D., Hernquist, L., et al. 2018, MNRAS, 475, 648
Poliakov, D., Mosenkov, A. V., Brosch, N., Koriski, S., & Rich, R. M. 2021, MNRAS, 503, 6059
Presotto, V., Girardi, M., Nonino, M., et al. 2014, A&A, 565, A126
Puchwein, E., Springel, V., Sijacki, D., & Dolag, K. 2010, MNRAS, 406, 936
Purcell, C. W., Bullock, J. S., & Zentner, A. R. 2007, ApJ, 666, 20
Ragusa, R., Mirabile, M., Spavone, M., et al. 2022, Front. Astron. Space Sci., 9
Ragusa, R., Spavone, M., Iodice, E., et al. 2021, A&A, 651, A39
Raj, M. A., Iodice, E., Napolitano, N. R., et al. 2020, A&A, 640, A137
Riess, A. G., Casertano, S., Yuan, W., et al. 2018, ApJ, 855, 136
Rudick, C. S., Mihos, J. C., & McBride, C. 2006, ApJ, 648, 936
Rudick, C. S., Mihos, J. C., Frey, L. H., & McBride, C. K. 2009, ApJ, 699, 1518
Rudick, C. S., Mihos, J. C., & McBride, C. K. 2011, ApJ, 732, 48
Sampaio-Santos, H., Zhang, Y., Ogando, R. L. C., et al. 2021, MNRAS, 501, 1300
Samurović, S. 2014, A&A, 570, A132
Schipani, P., Noethe, L., Arcidiacono, C., et al. 2012, J. Opt. Soc. Am. A, 29, 1359
Schlafly, E. F., & Finkbeiner, D. P. 2011, ApJ, 737, 103
Sommer-Larsen, J. 2006, MNRAS, 369, 958
Spavone, M., Capaccioli, M., Napolitano, N. R., et al. 2017, A&A, 603, A38
Spavone, M., Iodice, E., van de Ven, G., et al. 2020, A&A, 639, A14
Tempel, E., Kipper, R., Tamm, A., et al. 2016, A&A, 588, A14
Venhola, A., Peletier, R., Laurikainen, E., et al. 2017, A&A, 608, A142
Zhang, Y., Yanny, B., Palmese, A., et al. 2019, ApJ, 874, 165
Zwicky, F. 1937, ApJ, 86, 217
Zwicky, F. 1951, PASP, 63, 61
Zwicky, F. 1952, PASP, 64, 242
Zwicky, F. 1957, PASP, 69, 518